

Friction Force Microscopy Analysis of Self-Adaptive W–S–C Coatings: Nanoscale Friction and Wear

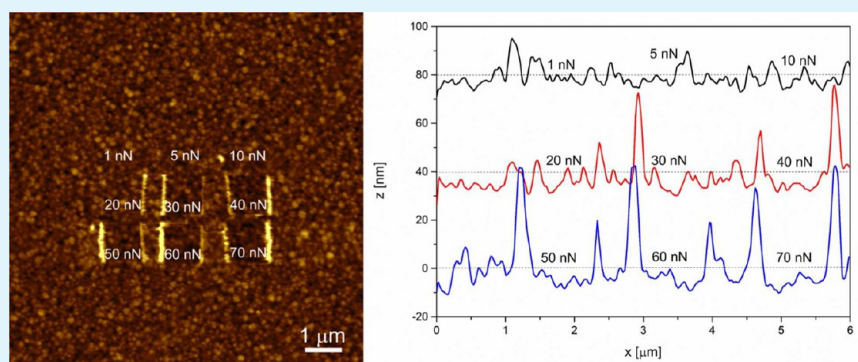
Jurgita Zekonyte^{*,†} and Tomas Polcar^{‡,§}

[†]School of Engineering, University of Portsmouth, Anglesea Building, Anglesea Road, Portsmouth PO1 3DJ, United Kingdom

[‡]National Centre for Advanced Tribology (nCATS), Faculty of Engineering and Environment, University of Southampton, Southampton SO17 1BJ, United Kingdom

[§]Department of Control Engineering, Faculty of Electrical Engineering, Czech Technical University in Prague, Technicka 2, Prague 166 27, Czech Republic

S Supporting Information



ABSTRACT: Transition metal dichalcogenides (TMD) are increasingly popular due to unique structural and mechanical properties. They belong, together with graphene and similar 2D materials, to a small family of solid lubricants with potential to produce ultralow friction state. At the macroscale, low friction stems from the ability to form well-oriented films on the sliding surface (typically up to 10 nm thick), with the TMD basal planes aligned parallel to the surface. In this study, we quantitatively evaluate tribological properties of three sputtered tungsten–sulfur–carbon (W–S–C) coatings at a nanoscale using friction force microscopy. In particular, we investigate possible formation of well-ordered tungsten disulfide (WS_2) layers on the coating surface. The coefficient of friction decreased with increasing load independently of coating composition or mechanical properties. In contrast, hard coatings with high tungsten carbide content were more resistant to wear. We successfully identified a WS_2 tribolayer at the sliding interface, which peeled off as ultrathin flakes and attached to AFM tip. Nanoscale tribological behavior of WSC coatings replicates deviation of Amonton's law observed in macroscale testing and strongly suggests that the tribolayer is formed almost immediately after the start of sliding.

KEYWORDS: atomic force microscopy, X-ray photoelectron spectroscopy, nanoscale friction, nanowear, magnetron sputtering, tungsten–sulfur–carbon coatings, self-adaptive coatings

1. INTRODUCTION

Solid lubricants are materials that can exhibit very low friction during sliding in the absence of external supply of lubricant. Transition metal dichalcogenides (TMD) belong to one of the most developed classes of materials for solid lubrication, with molybdenum disulfide (MoS_2) being the most studied material, showing superlow friction sliding in high vacuum.^{1–4} Low friction stems from the ability to form an oriented film on the sliding surface, with the basal planes aligned parallel to the surface, due to low adhesion and shear strength between the planes.⁵ At the nanoscale, a rotational disorder is expected between the planes in order to decrease dissipated energy and thus friction (incommensurate sliding).⁴ One of the main drawbacks of pure TMD coatings (typically prepared by magnetron sputtering) is their low load-bearing capacity and

limited wear resistance. To remedy this lack, TMD coatings were codeposited with nonmetallic interstitial elements such as carbon, producing coatings such as tungsten–sulfur–carbon (W–S–C) and molybdenum–selenium–carbon (Mo–Se–C) which showed an enhanced mechanical resistance with improved tribological properties. Yet they still possessed solid lubricant properties due to their unique self-adaptive behavior.^{6–11} During sliding of these coatings, a thin TMD tribolayer (up to 10 nm) with well-ordered planes parallel to the sliding direction is produced. The tribolayer simultaneously

Received: March 24, 2015

Accepted: September 4, 2015

Published: September 4, 2015

protects the coating from environmental attack and provides low friction.

Friction (or lateral) force microscopy (FFM) is often used to study nanoscale tribological properties of lamellar-like solid lubricants such as niobium diselenide (NbSe_2), molybdenum oxide (MoO_3), molybdenum disulfide (MoS_2), graphite, and graphene, as well as nonlayered carbon-based solids.^{12–15} Most of the studies concentrate on friction measurements in the elastic regime, i.e. below the critical load at which observable damage might take place. Yet, plastic deformation is integral part of the majority of sliding contacts, and thus material wear is an unavoidable process. Atomic wear by FFM was reported for lamellar-like materials, including mica,^{16–19} single-crystal calcite,²⁰ potassium bromide (KBr),²¹ as well as NbSe_2 and MoS_2 .^{22,23} The mechanism of material wear was shown to be dependent on environmental conditions, applied load, and materials properties. For example, the wear of layered materials, such as mica, MoS_2 or NbS_2 , occurs in a relatively controlled layer-by-layer manner.^{16,17,19,22} After a critical number of surface defects is accumulated during tip sliding, AFM produces a visible wear scar. The removal and rearrangement of single ionic pairs is the main mechanics of KBr surface wear.²¹ The debris generated during scratching forms layers that rearrange in an epitaxy-like process with the orientation and periodicity as the underlying substrate. All the above-reported FFM studies were carried out on materials with well-defined crystallographic and/or layered structures. In contrast, TMD based coatings, such as W–S–C, prepared by magnetron sputtering exhibit complex structure combining amorphous and crystalline phases, and well-ordered tribolayer is formed during traditional pin-on-disc tribological experiments.^{6,10} In our previous FFM study²⁴ on chromium-doped W–S–C coatings, we concentrated on the nanoscale friction properties at low loads in the elastic regime. Very low levels of wear were observed, but this was attributed to the removal of surface contamination. As single-pass for each load was carried out, no topographical changes were identified, and therefore the formation of the tribolayer was not observed.

The purpose of this study is to evaluate tribological properties at the nanoscale, and identify if well-ordered tungsten disulfide layers can be formed on W–S–C coatings using friction force microscopy. The results are analyzed as a function of coating's chemistry and mechanical properties.

2. EXPERIMENTAL SECTION

2.1. Coating Preparation and Characterization. The W–S–C films were deposited using a direct current (d.c.) magnetron sputtering (chamber fabricated by Teer, U.K.) onto Si wafers (hereinafter, "substrates"). Prior to the coating deposition, the substrates were cleaned by establishing the argon plasma close to the substrates. Cleaning process parameters were as follows: argon pressure, 1.5 Pa; substrate bias, -600 V; cleaning time, 30 min. Four targets were used: chromium (purity 99.9%), two graphite targets (graphite, purity 99.6%), and one WS_2 target (purity 99%). After the plasma etching, the substrates were coated first with a thin (approximately 250 nm) bonding layer consisting of pure Cr and a gradient Cr/W–S–C layer with decreasing Cr content; the argon pressure was 0.3 Pa, and substrate bias of -50 V was applied. Finally, the W–S–C coating was deposited at a pressure of 0.45 Pa (substrate was grounded, and bias was not applied) using two graphite and one WS_2 targets. Different chemical composition was achieved by changing target-to-substrate distance. Three distances (30, 23, 15 mm) were used to vary final chemical composition; the coatings were then denominated as WSC-A, WSC-B, and WSC-C, respectively. Decreasing distance from target resulted in a higher sputtering of sulfur from coating surface by

reflected argon atoms from the target. The thickness of the coatings, measured through film cross-section using secondary electron microscopy (SEM), was 1000–1100 nm.

The chemical analysis of deposited coatings was done using X-ray photoelectron spectroscopy (XPS; Thermo Scientific Theta Probe XPS, U.K.). Survey and core level XPS spectra were obtained with a monochromatized Al $K\alpha$ radiation ($h\nu = 1486.7$ eV) using 400 μm spot size. XPS was carried out before and after surfaces were sputter cleaned with 1 keV Ar^+ ions for 30 s, ion current 1 μA , irradiated area of 2×2 mm. Spectra were analyzed using Thermo Avantage software (Thermo Fisher Scientific, U.K.). Curve fitting was done using a Gaussian–Lorentzian (70–30) function.

Mechanical properties (hardness (H) and reduced modulus (E_r)) were determined using depth-sensing nanoindentation technique (NI) (Nano Test Vantage from Micro Materials, U.K.).²⁵ Indentations were done with Berkovich tip in a load controlled mode. The maximum load was set to 1.2 mN so that the maximum displacement would not exceed 100 nm, loading/unloading rate 0.1 mN/s, dwell time at maximum load -20 s. At least 15 indents were placed on each coating. Data were analyzed using the Oliver–Pharr method²⁶ with an analytical software provided by Micro Materials.

2.2. Friction Measurements Using AFM. Surface topography and lateral force measurements were done in air at room temperature using atomic force microscope (MAC Mode III, 5500 Scanning Probe Microscopy, Agilent Technologies, Santa Clara, CA). PicoView 1.12 and PicoImage Basics 6.0 (Agilent Technologies, Santa Clara, CA) software were used for data acquisition and image analysis, respectively. Standard force modulation silicon probes (NanoWorld, distributed by Windsor Scientific, U.K.) with nominal spring constant of 2 N/m and tip radii of 8–10 nm were used. Actual spring constant values for every cantilever were obtained using built-in thermal noise method.²⁷ The determined constant varied between 1.8 and 2.2 N/m. Normal forces were calibrated by measuring the deflection sensitivity (nm/V) from the slope of the linear part of a force–displacement curve obtained on a flat silicon surface. The normal force, F_N , was set to be zero at the point where the cantilever left the surface. Calibration of lateral forces, using commercially available gratings, was achieved employing the "wedge calibration method" according to Ogletree et al.²⁸ The probe geometry before and after experiments was analyzed by SEM.

For the friction and wear measurements, the instrument was operating in contact mode with the long cantilever axis perpendicular to scanning direction. The lateral deflection was adjusted so that it was zero with the tip out of contact with the surface. To determine friction properties of coatings as a function of applied load, we recorded topography and friction maps over areas of $4 \times 4 \mu\text{m}$ consisting of 512 lines at a scanning speed of 8 $\mu\text{m/s}$ (1 line/s). The load was increased from 0.5 to 300 nN with a step of 5–10 nN every 100 nm, ensuring that at least 12 lines were attributed to one load. At least three scans at different locations were carried out. Friction forces were determined from trace–retrace loops acquired along single lines by subtracting and halving mean signals as described in ref.²⁹ Wear experiments were done over areas of $1 \times 1 \mu\text{m}$ at a scanning speed of 3.99 $\mu\text{m/s}$ (2 lines/s), applied loads were 10, 50, 100, and 300 nN. Up to 100 frames were recorded for each load. To monitor coating wear, we increased frame size to $3 \times 3 \mu\text{m}$ and reduced the load to 0.5 nN between runs. Material volume loss was calculated from topographical images. Surface area roughness of each sample was determined over the frame size of $10 \times 10 \mu\text{m}$ using PicoImage software. Mean surface roughness, S_a (arithmetic mean height deviation), related to the analysis of three dimensional (3D) areal surface texture, was calculated according to ISO 25178 standard using Gaussian filter 0.008 mm.

3. RESULTS AND DISCUSSION

3.1. Coating Composition and Mechanical Properties. Three series of coatings were deposited with different tungsten (W), sulfur (S), and carbon (C) content. The chemical composition of the surface, and relative percentages of WS_2 , WC, and W_xO_x related bonds are given in Table 1. Surface

Table 1. XPS Surface Chemical Composition of the Coatings after Cleaning with Ar⁺ Ions

WSC surface stoichiometry		chemical composition (atomic %)				relative percentages (relative atomic %) ^a			
		W	S	C	O	WS ₂	WC	WO ₃	rest
A	WO _{0.26} S _{0.97} C _{0.63}	35	34	22	9	29	27	14	30
B	WO _{0.27} S _{0.81} C _{0.62}	37	30	23	10	27	32	15	26
C	WO _{0.12} S _{0.56} C _{0.65}	43	24	28	5	24	53 ^b	9	14

^aRelative percentages of WS₂, WC, WO₃ related bonds and the rest features (C–C, C–O, O–S) present in the films were calculated from W 4f, S 2p, C 1s, and O 1s spectra and chemical composition. ^bAbout 4% could be attributed to metallic tungsten.

composition of samples A and B were found to be similar with a small decrease in sulfur content for WSC-B, as indicated by elemental stoichiometry, while evident reduction in oxygen and sulfur was measured for WSC-C. The reported data were obtained after the Ar⁺ ion sputter cleaning required to reduce the effect of contamination. The atomic concentrations of C and O decreased by half after the cleaning, whereas the concentration of W and S increased (Supporting Information, Figure S1). Additionally to the removal of organic contamination, ion etching typically leads to the preferential sputtering of sulfur.³⁰ This might result in lower sulfur amount on the surface when compared to the bulk of the coating. Rumaner et al.³⁰ demonstrated that sulfur content rapidly decreased within ion dosages $1 \times 10^{15} - 5 \times 10^{16}$ ions/cm², when WS₂ single crystals were sputtered in the energy range 150–1000 eV. The final surface composition was measured \sim WS_{0.4}. The total ion dose used in our experiments was about 4×10^{15} ions/cm². Following Rumaner et al.,³⁰ the ratio between W and S should be approximately 1:1.5. Taking into account that our coatings contained additional elements such as carbon and oxygen, and the aim was to prepare films with varying elemental composition, the resulting surface stoichiometry was expected to deviate from the ideal one.

Relative concentrations of WS₂, WC, and WO₃ were calculated from W 4f, S 2p, C 1s, and O 1s core peaks (Supporting Information, Figure S1; detailed XPS spectra analysis and discussion) and surface chemical composition (Table 1). Mullins and Lyman³¹ demonstrated that with increasing sulfur coverage, WS₂ is formed. In our calculations, we have ignored preferential sulfur loss during ion cleaning process, and have assumed that one tungsten atom bonded to two sulfur atoms. The results showed that with increasing carbon and decreasing sulfur contents, the amount of tungsten carbide (WC) increased with respect to WS₂ and tungsten oxide (WO₃). Furthermore, for the WSC-C sample, \sim 4% from the WC concentration could be attributed to metallic tungsten, as W 4f spectrum was shifted toward lower binding energies. Please note that prepared coatings did not consist purely of WS₂, WC and WO₃, because of the presence of various S–O, C–O, and C–C bonds. Their contribution decreased with decreasing oxygen amount.

Hardness (*H*) and reduced modulus (*E_r*) of the films, measured using nanoindentation instrument, are reported in Table 2. The mechanical properties of the films increased in the following order: WSC - A < B < C, i.e. the higher WC content, the harder was the coating. Therefore, it is expected that wear resistance will follow the same trend, while the ability to form well-ordered WS₂ layers^{6–8} during the sliding would retain low friction coefficient. Surface topography of the coatings measured with AFM is given in Figure 1. Corresponding areal surface roughness is presented in Table 2. Coatings with higher WC content exhibited larger columnar structures and slightly rougher surfaces.

Table 2. Properties of the Coatings^a

WSC	mechanical properties			
	<i>H</i> (GPa)	<i>E_r</i> (GPa)	Sa (nm)	τ (MPa)
A	4.9 ± 0.31	60.0 ± 2.49	2.05 ± 0.15	36 ± 5
B	6.3 ± 0.43	70.3 ± 2.89	2.66 ± 0.12	83.4 ± 3
C	7.6 ± 0.61	86.7 ± 4.11	3.26 ± 0.17	91.2 ± 3

^aHardness (*H*) and reduced modulus (*E_r*) were obtained by nanoindentation; areal surface roughness (Sa) from AFM analysis; and interfacial shear strength, τ , calculated from FFM-AFM results for tip radius of 20 nm.

3.2. Single Scan Nanofriction As a Function of Load.

AFM based tribological measurements are usually done in the elastic regime, below the threshold load for observable damage to take place. The existence of the critical load will depend on the materials under the investigation, and experimental condition employed. The friction response was recorded as a function of applied load, which was gradually increased up to 300 nN. Friction force, *F_f*, as a function of normal load, *F_N*, for the three coatings obtained with FFM during the single scan is given in Figure 2 for WSC-B and WSC-C, and Figure 3 for WSC-A. Two distinct behaviors were observed between the softer WSC-A coating and the two harder WSC-B and WSC-C coatings, as discussed in the following chapters.

3.2.1. Nanofriction of WSC-B and WSC-C Films. Friction force dependence on the applied load for WSC-B and WSC-C coatings is given in Figure 2. As predicted by several continuum models of the elastic contact in the single asperity regime, all coatings exhibit a nonlinear dependence between friction force and normal loads, especially in the low applied load region. The models assume that the lateral (or friction) force is proportional to contact area, *A*:^{32–36}

$$F_f = \tau A \quad (1)$$

where τ is the interfacial shear strength. The nonlinearity stems from the contact area dependence on the external load, *F_N*, which for a nonadhesive Hertzian contacts, $A \propto F_n^{2/3}$.^{34,37–39}

$$A_{\text{Hertz}} = \pi \left(\frac{R}{K} \right)^{2/3} F_n^{2/3} \quad (2)$$

where *R* is the radius of the tip, and *K* the effective elastic modulus of the contact.

$$K = \frac{3}{4} \left(\frac{1 - \nu_1^2}{E_1} + \frac{1 - \nu_2^2}{E_2} \right)^{-1} \quad (3)$$

where ν_i is Poisson's ratio, and *E_i* is the Young's moduli of the sphere and flat surface.

However, attractive forces between the tip and the sample are always present. The effect of adhesion was included in other models: Johnson–Kendall–Roberts (JKR)⁴⁰ for the attractive forces acting inside the contact area, Derjaguin–Muller–

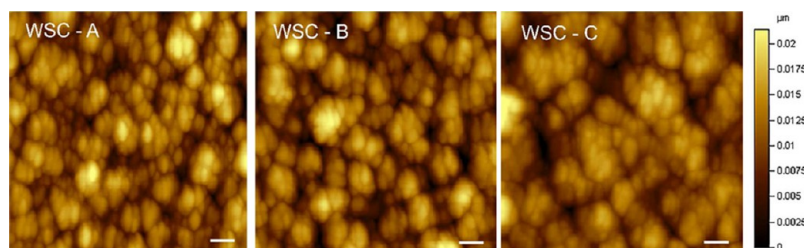


Figure 1. AFM topography images for WSC – A, B, and C coatings. Image size: $1 \times 1 \mu\text{m}$. Scale bar: 100 nm.

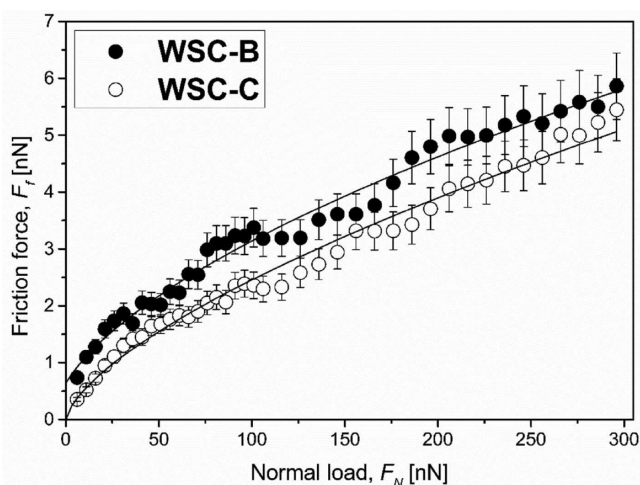


Figure 2. Average results of friction force as a function of load for WSC-B and WSC-C coatings. Data were fitted to Hertz-plus-offset model, eq 4.

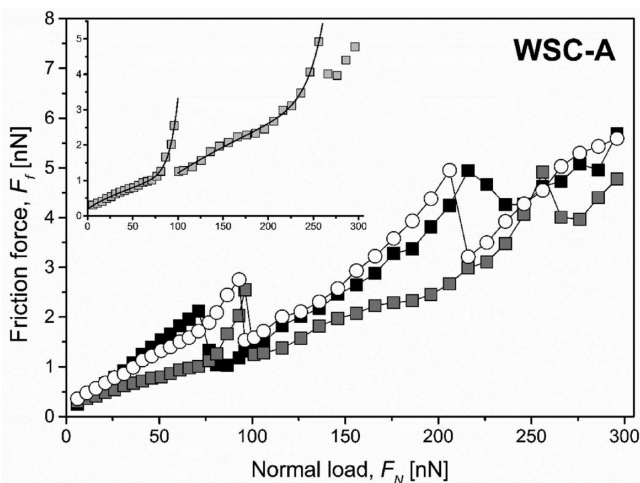


Figure 3. Friction force as a function of load for WSC-A coating measured with FFM. The inset shows the fit to eq 5 to one of the curves.

Toporov (DMT)³⁷ for the attractive forces that act predominantly outside the contact area. In reality, most cases fall between those two models. Simple JKR–DMT transition theories based on the Maugis–Dugale³⁸ model were proposed by Carpick–Olegtree–Salmeron (COS)³² and later justified by Schwarz.⁴¹ Our results for WSC-B and WSC-C coatings (Figure 2) were fitted to modified DMT–Maugis theory, also known as the Hertz-plus-offset model.^{36,41} The model states that a spherical tip elastically deforms a flat surface, while the additional adhesive forces are indirectly introduced via the

increasing value of A . It was also shown that the actual contact area would be proportional to the load and would depend on the shape of the tip: in Hertzian case the contact area is proportional to $F_n^{2/3}$, while for pyramidal or conical tips to $F_n^{1/2}$.^{35,36} The dependence of contact area versus load can be approximated as $A \sim F_n^m$, with $0 < m < 1$ for low loads (consequence of undefined tip/sample contact). With the additional fitting parameter m , the Hertz-plus-offset model takes the following form:

$$F_f = \tau A = \tau \pi \left(\frac{R}{K} \right)^m (F_N - F_{\text{off}})^m = C (F_N - F_{\text{off}})^m \quad (4)$$

where $C = \tau \pi (R/K)^m$ is the constant in units adequate to m , F_N is an effective force acting between the surface and the sphere and is the sum of the applied load and the adhesive forces ($F_N = F_n + F_{\text{ad}}$), F_{off} is the constant offset caused by adhesion and should be lower than measured adhesion force.³⁶ The best fit to eq 4 was obtained when $m = 0.600 \pm 0.04$, $C = 0.126 \pm 0.014 \text{ nN}^{(1-m)}$, and $F_{\text{off}} = -1.9 \pm 0.04 \text{ nN}$ for WSC-B; and when $m = 0.664 \pm 0.04$, $C = 0.114 \pm 0.032 \text{ nN}^{(1-m)}$, and $F_{\text{off}} = 0.082 \pm 0.05 \text{ nN}$ for WSC-C. Adhesion (pull-off) forces determined from load–displacement curves before and after experiments changed only by few nN, from $4 \pm 0.5 \text{ nN}$ to $6\text{--}7 \pm 0.7 \text{ nN}$. The very small deviation from 2/3 power law in our case, could be due to the change of the tip geometry,^{42,43} different area-load dependence because of the different surface microstructure,³⁵ or the possibility to undergo surface structural and chemical changes under high pressure.⁴⁴ It was demonstrated by several researchers^{42,43} that sharp AFM tips fractured almost immediately upon the first engagement with the hard surface, reached “semiconstant” radius of $\sim 20 \text{ nm}$ within the first 10 mm of scanning distance, and remained constant for about another 100 mm. Even if the tip wear increased with the load, the wear process was slow because it occurred atom by atom.⁴⁵ During this particular experiment, the total scanning distance for each tip was about 30 mm, from which three cycles of 4.1 mm were subjected to the increase in load from 0 to 300 nN. Considering reported findings and our observation from earlier work,²⁴ we assume that the “stable” tip radius of 20 nm was reached during the acquisition of the force–displacement curves before friction experiments, and during the first few images at low loads. It was supposed that the tip shape remained constant for the duration of these particular experiments. Most likely, the fracture in AFM tip during the first interactions with the surface resulted in the final tip geometry that was not an ideal sphere, hence the deviation from 2/3 power law.

Assuming that AFM tip radius was 20 nm for the duration of the single scan friction experiments, then interfacial shear strength, $\tau = C' K^m / \pi R^m$, yielded $\sim 83.8 \text{ MPa}$ for WSC-B and 91.2 MPa for WSC-C (Table 2). The present results are similar

to those reported on WSC coatings doped with Cr²⁴. Shear strength for pure WS₂ is not known, as most published works are for MoO₃ and MoS₂. Shear strength of MoS₂, which is expected to be slightly lower, was measured in the range of 23–33 MPa² using macroscopic measurement techniques. Wang et al.⁴⁶ measured shear stress by AFM-FFM between MoO₃ particles and MoS₂ surface. Reported values were in the range of 40–940 MPa, where the shear stress decreased with increasing particle size. Considering similar crystal structure and frictional properties of MoS₂ and WS₂, we assume that easy-shearing WS₂ tribolayer can be formed on the coating surface during the nanoscale measurements.

Surface roughness of our samples should not influence frictional measurements. Recently published works^{47–49} indicated that friction did not depend on surface roughness amplitude, or the height of the surface nanotextures, but rather showed some relation to the slope of the local corrugation.

3.2.2. Friction Properties of WSC-A. While monitoring friction force response to the applied load for WSC-A sample (Figure 3), the sudden increase in the friction force and then abrupt drop in the load range of ~80–100 nN and ~200–250 nN was measured for every independent scan.

Several studies on mica reported the existence of a threshold load at which the immediate surface damage occurs. It was suggested, that a critical number of point defects was generated during the AFM tip sliding resulting into the nucleation of a hole, and the wear occurred in a layer-by-layer manner.^{16,17,19} Kopta and Salmeron¹⁷ proposed the following friction force dependence:

$$F_f = C(F_N - F_{\text{off}})^{2/3} + A_0 F_N^{2/3} e^{B_0 F_N^{2/3}} \quad (5)$$

where the first term includes the wearless friction part proportional to the contact area following Hertz-plus-offset model. The second term is the contribution of the defect production model, where additional friction force is assumed to be proportional to the number of defects produced in the contact area, and A_0 and B_0 are constants. The fit to eq 5 is shown in the inset of Figure 3 for one of the curves. The interfacial shear strength, τ , recalculated from the first term of eq 5 for a tip radius of 20 nm, was $\sim 36 \pm 5$ MPa. The low value of τ suggests that WSC-A film might form well-ordered tribolayer easier than WSC-B and C coatings.

If applied load in the range of 80–100 nN indicates the threshold above which surface wear occurs, what is the origin of “friction spikes” observed at high loads? W–S–C type coatings form well-ordered WS₂ layers during tribological tests even at the nanoscale. And we expect that the mechanism of wear of these coatings is layer-by-layer. The drop in F_f after reaching high value is a consequence of the removal of the top layer, and the exposure of the new underlying surface. New defects have to be generated on the new layer to progress surface wear, thus the second increase and drop in F_f at high loads. The analysis of topography images (not shown here) did not indicate any visible changes. Even though the surface roughness of the films is just few nanometers, it is still too rough, and AFM resolution does not allow the identification of the formation of point defects after one scan.^{17,19,21,22} Even if nanotribological measurements were run at loads above 100 nN, at least 4 scan cycles were required to measure visible changes on atomically flat mica.^{17,19} Therefore, multiple scans should be done before any AFM visible changes can be recorded.

Nanowear of surfaces can occur even at lower loads, provided that multiple scanning was run at the same place.^{16–19,21–23}

3.3. Nanowear: Tribological Response to Multiple Scanning. To measure wear and investigate the possible formation of WS₂ tribolayer, each sample was subjected to multiple scans at loads 10, 50, 100, and 300 nN. Up to 100 frames of the size $1 \times 1 \mu\text{m}^2$ were recorded for each load. The average results of the coefficient of friction (COF) obtained during wear experiments for three samples are shown in Figure 4. COF decreased with increasing load, which is usual behavior

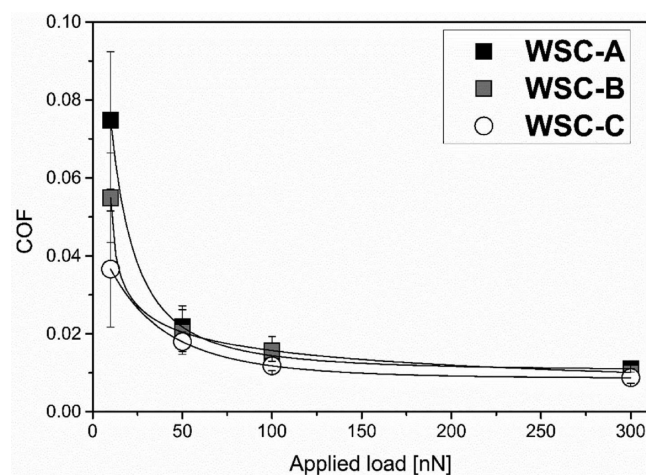


Figure 4. Coefficient of friction measured for three coatings with FFM-AFM during wear experiments.

for TMD and TMD-based coatings, such as MoS_x, WSC, MoSeC^{2,6,7,10,50} and some polymers.⁵¹ Typically, friction coefficient is either independent of load or increases with load. Labuda et al.⁵² showed that the friction of Au (111) measured by AFM is almost constant in the load range of 0–5 nN, whereas the friction of gold oxide sharply increased. Graphene tested as single sheet or in bilayer form exhibited small increase in friction with increasing load.⁵³

The coefficient of friction for the three WSC coatings did not differ greatly, and did not show dependence on coating chemistry or mechanical properties. The only larger difference in COF was measured at 10 nN load. It was argued,³³ that softer materials will give rise to a larger contact area for the equivalent load, thus leading to the higher frictional force measured at the nanoscale. WSC-A coating is the softest of all three (Table 2), so if friction force according to the single asperity theories is proportional to the contact area (eq 1), it stands to reason for this coating to have the higher COF. At higher loads, the apex of the tips used on harder surfaces should blunt faster forming larger radius. This would lead to the increase in the contact area, and similar COF values. Material transfer from the sample surface to AFM tip will contribute to the change in the tip radius, and alter counterpart chemistry, thus affecting friction properties.

3.3.1. Layer-by-Layer Wear and Easy-Shear Layer Formation for WSC-A. Material wear is accompanied by the material transfer between the tip and the substrate. The mechanism and amount of transferred material will depend on material properties, applied load, and environment. An increase/decrease cycles of F_f were measured as a function of frame number. Figure 5a shows the results for WSC-A coating. At 10 nN load, a continuous increase in friction was measured

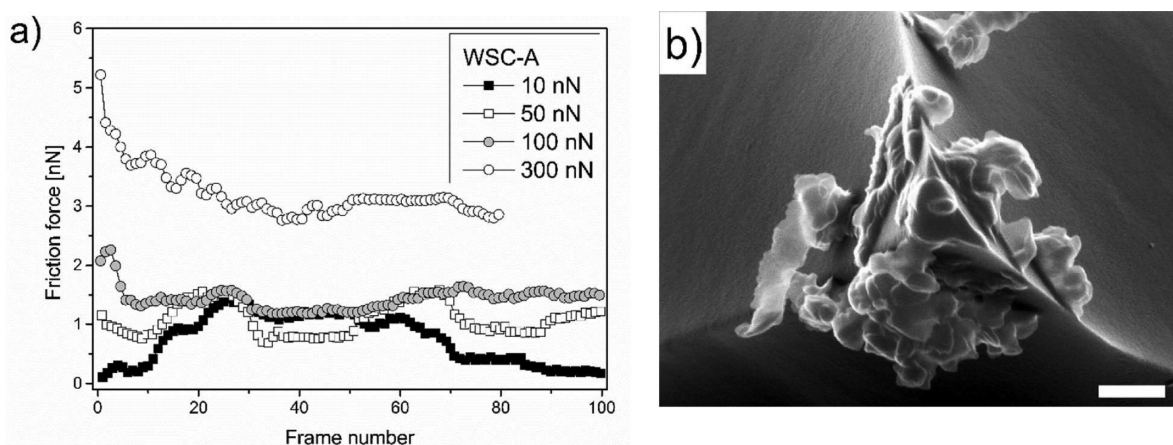


Figure 5. a) Friction force as a function of frame number measured with FFM during wear experiments for WSC-A. (b) SEM image of the AFM tip after wear experiments at 300 nN. Image was acquired with acceleration voltage of 15.0 kV; at magnification $\times 55,000$; scale bar: 250 nm.

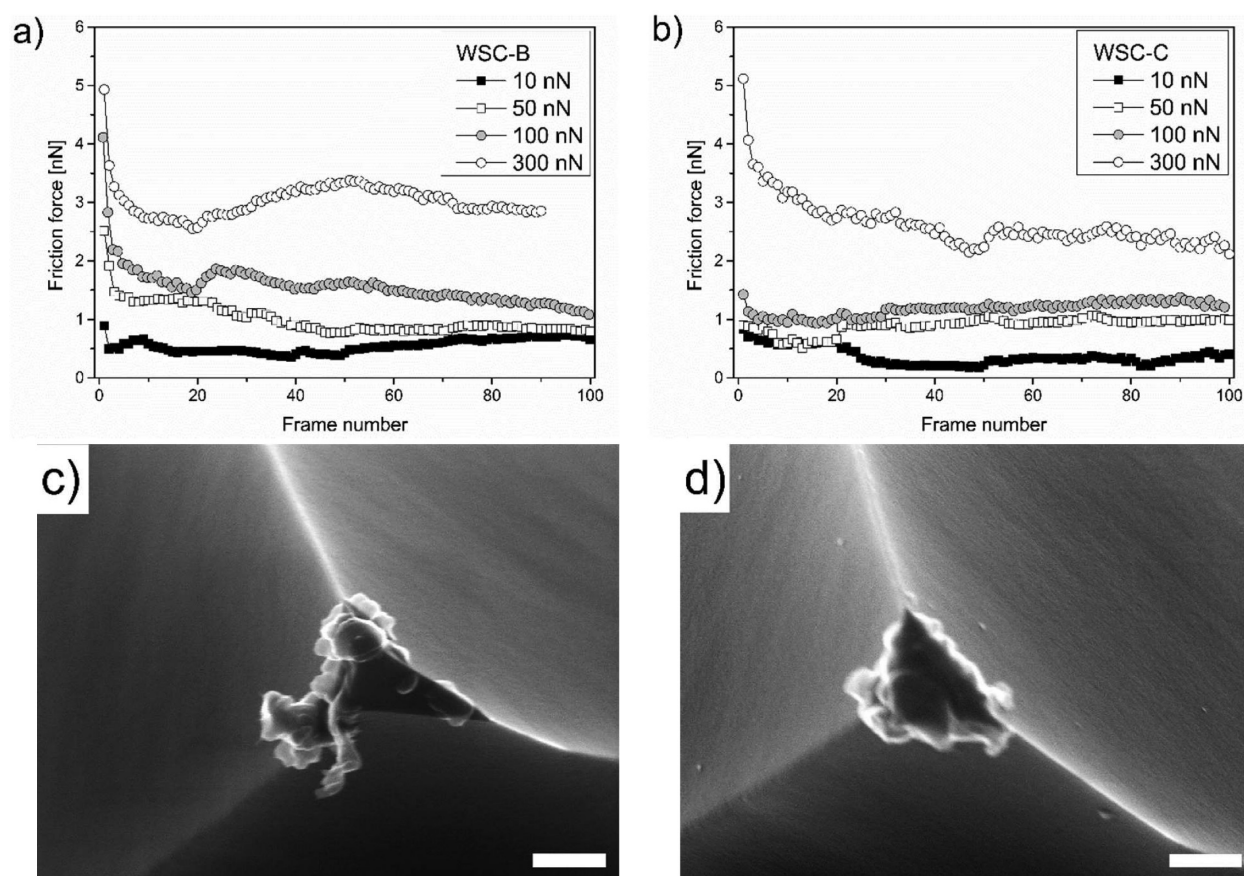


Figure 6. Friction force as a function of frame number measured with FFM during wear experiments for (a) WSC-B, and (b) WSC-C coatings. SEM images of AFM tips after wear experiments at 300 nN on samples (c) WSC-B, and (d) WSC-C. Images acquired with acceleration voltage of 15.0 kV; at magnification $\times 55,000$; scale bar: 250 nm.

for up to 25–30 frames, then a relatively constant plateau was obtained for another 30 frames followed by the decrease to the initial friction force values. The increase in friction can be due to several factors. First, tip wear occurs during continued scanning, resulting in an increase in tip radius, contact area and frictional force. Second, an increase in friction force with multiple scanning is related to the generation of critical number of surface defects responsible for the removal of surface layers. Finally, the surface is gradually modified during the repetitive scanning resulting in a complete structural change. AFM

topography images showed that during the initial 20–25 frames, surface features became larger, and not so clearly distinguishable. During the continuous scanning, surfaces undergone structural changes losing columnar/grain type morphology. The surface was covered with “amorphous”, “liquid-like” film (Supporting Information, Figures S2 and S3). The drop in friction force at prolonged scanning is attributed to the delamination of created tribolayer and the exposure of the surface underneath it.

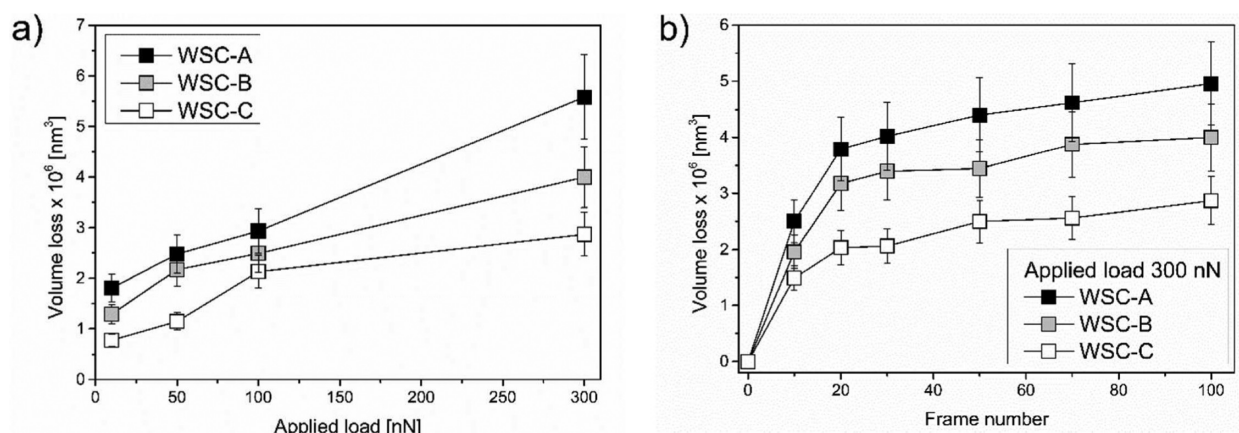


Figure 7. (a) Total volume loss of coating material during wear test as a function of a load. (b) Volume loss as a function of frame number for wear test at load of 300 nN.

The breakage of newly formed layer during tip sliding was observed for experiments carried out at load of 50 nN. Two cycles of friction force increase/decrease were recorded, Figure S_a, with the interval much shorter than that for 10 nN load. The first shear layer was formed between frames 10 and 25. After the first layer was removed, an underlying surface was revealed showing relatively clear topographical structure between frames 30 and 50 (Support Information, Figures S2 and S3). Then the same process was repeated again, i.e. formation of new tribolayer followed by its removal. Measured areal surface roughness, S_a , values fluctuated from $\sim 0.5 \pm 0.05$ nm for the frames indicating shear film formation to 0.95 ± 0.05 nm for the newly exposed surfaces. These results indirectly prove the removal of tribofilm and exposure of the underlying surface. Similar changes were observed for a load of 100 nN. Interestingly, the above-mentioned behavior is not clear for 300 nN load. The results showed that the surface was modified during the first 10 scans. But topography did not alter significantly for the rest of the test, although the wear of the material was observed (Supporting Information, Figures S2 and S3). To prove that topography was completely altered within the $1 \mu\text{m}^2$ wear test frame due to morphological changes under the pressure, a zoom-out image of $3 \mu\text{m}^2$ was recorded with the same tip immediately after each wear test. The wear scars were surrounded by columnar structures, while the modified area showed the lack of any defined structure (Supporting Information, Figure S6).

AFM tip after wear test on WSC-A was analyzed using SEM, Figure S_b. It proves that WSC-A coating wear occurs in layer-by-layer fashion, and the easy shear layers are formed during FFM-AFM experiments. During the nanowear experiments a well-ordered layer in the form of ultrathin flakes is transferred to the tip. Every subsequent material transfer pushed previous layer further away from the apex, until an accumulation of several sheets become firmly attached to the tip, producing the surface with low friction material. Energy-dispersive X-ray spectroscopy (EDS) elemental analysis of transferred material indicated the presence of Si and O₂ (that are the main elements of the AFM tip), and W and S₂ with approximate atomic ratio of W:S = 1:2.2 suggesting the formation of WS₂ during the sliding.

In summary, it takes longer to form the shear layer at low loads, but it is stable for a longer time/sliding distance that is required to accumulate surface defects to break the layer.

During intermittent loads, the tribolayer is created faster, but it is also removed faster starting another formation cycle. Finally, tribolayers are created rather fast at high loads and remain stable for a long time, which is probably because the tribofilm is firmly attached to the AFM tip at high contact pressures.

3.3.2. Nanowear of WSC-B and WSC-C Coatings. Friction force dependence as a function of frame number for WSC-B and WSC-C coatings did not show any difference up to 300 nN load, Figure 6a. In general, stable F_f values for both coatings were obtained after surfaces were subjected to about 5 to 10 scans. The decrease in friction force during the first scans was attributed to the removal of superficial contamination and oxidation, as no significant topographical changes within this scanning range were observed.

The formation of the shear layer for WSC-B sample was observed only at load of 300 nN, after ~ 40 – 50 scans (Supporting Information, Figures S4 and S5). The presence of the tribofilm is also confirmed in Figure 6c, where sheets similar to those obtained for WSC-A sample were transferred to the tip apex. It was rather difficult to determine when shear layers started to form on WSC-C coating, since it was neither directly indicated in friction force measurements (Figure 6b) nor in AFM height images (Supporting Information, Figures S4 and S5). WSC-C coating was also transferred to the tip forming a “ball” with a very large radius, Figure 6d. Unlike for WSC-A or WSC-B samples, the “ball” stayed firmly attached to the tip apex during the sliding experiments resulting in the AFM image distortion (Supporting Information, Figures S4, S5 and S6). EDS analysis confirmed that transferred layer contained tungsten and sulfur. Even though AFM topographical results cannot visually confirm the appearance of WS₂ type layers for WSC-C coating, the decrease in friction indicates the presence of such low-shear tribolayers. We can conclude here that frictional behavior measured by FFM is similar to that observed in the macroscopic tribological tests.^{8,10}

Finally, Figure 7 shows the material loss during wear experiments calculated from AFM profile images (Supporting Information, Figure S6). As expected, the wear is higher for WSC-A coating followed by WSC-B and WSC-C. The example of volume loss as a function of sliding distance is given in Figure 7b for the load of 300 nN. The first measurable wear of the coating occurs during the first 10–20 scans, and reaches almost constant wear after a few more frames. The same tendency was observed at all loads. In general, the wear of

coatings increased with the applied load but decreased as a function of time or sliding distance.

4. CONCLUSIONS

Tribological properties of solid lubricant W–S–C coatings with various chemical composition and mechanical properties were analyzed at the nanoscale. Distinct behavior was observed between the softer WSC-A coating and the two harder WSC-B and WSC-C coatings. For WSC-A coating, friction force dependence on applied load during the single scan experiments indicated the presence of a threshold load ~ 100 nN, at which immediate surface deformation occurs. Nanowear experiments of this material indicated the formation of ultrathin shear layers during continuous tip sliding over the sample surface below and above the measured load threshold. Coating wear at the nanoscale took place in a layer-by-layer fashion. The speed at which the tribolayer was formed and its stability depended on the applied load.

Nonlinear friction force dependence on applied load, measured for hard coatings WSC-B and WSC-C, follows the single asperity model of elastic contact (Hertz-plus-offset model). The first indication of tribolayer formation for WSC-B coating was observed at the highest load of 300 nN. No AFM visible tribofilm was generated on the WSC-C coating for the experimental conditions employed, although W–S based material was observed to transfer to the AFM tip.

Wear of coatings increased with the applied load, but decreased as a function of time/sliding distance. Coatings with higher tungsten carbide content showed better wear resistance while retaining low friction properties.

■ ASSOCIATED CONTENT

Supporting Information

The Supporting Information is available free of charge on the ACS Publications website at DOI: 10.1021/acsami.5b05546.

Additional information on XPS core level spectra analysis, AFM topographical changes during nanowear experiments, and profiles. (PDF)

■ AUTHOR INFORMATION

Corresponding Author

*E-mail: jurgita.zekonyte@port.ac.uk Tel.: +44 (0) 23 9284 2330.

Author Contributions

The manuscript was written through contributions of all authors. All authors have given approval to the final version of the manuscript. All authors contributed equally to this work.

Notes

The authors declare no competing financial interest.

■ REFERENCES

- (1) Hirvonen, J. P.; Koskinen, J.; Jervis, J. R.; Nastasi, M. Present Progress in the Development of Low Friction Coatings. *Surf. Coat. Technol.* **1996**, *80*, 139–150.
- (2) Singer, I. L.; Bolster, R. N.; Wegand, J.; Fayeulle, S.; Stupp, B. C. Hertzian Stress Contribution to Low Friction Behavior of Thin MoS₂ Coatings. *Appl. Phys. Lett.* **1990**, *57*, 995–997.
- (3) Singer, I. L.; Fayeulle, S.; Ehni, P. D. Wear Behavior of Triode-Sputtered MoS₂ Coatings in Dry Sliding Contact with Steel and Ceramics. *Wear* **1996**, *195*, 7–20.
- (4) Martin, J. M.; Donnet, C.; Lemogne, T.; Epicier, T. Superlubricity of Molybdenum-Disulfide. *Phys. Rev. B: Condens. Matter Mater. Phys.* **1993**, *48*, 10583–10586.

- (5) Dominguez-Meister, S.; Conte, M.; Igartua, A.; Rojas, T. C.; Sanchez-Lopez, J. C. Self-Lubricity of WSe₂ Nanocomposite Coatings. *ACS Appl. Mater. Interfaces* **2015**, *7*, 7979–7986.

- (6) Polcar, T.; Cavaleiro, A. Review on Self-Lubricant Transition Metal Dichalcogenide Nanocomposite Coatings Alloyed with Carbon. *Surf. Coat. Technol.* **2011**, *206*, 686–695.

- (7) Polcar, T.; Evaristo, M.; Cavaleiro, A. Comparative Study of the Tribological Behavior of Self-Lubricating W–S–C and Mo–Se–C Sputtered Coatings. *Wear* **2009**, *266*, 388–392.

- (8) Polcar, T.; Evaristo, M.; Cavaleiro, A. Self-Lubricating W–S–C Nanocomposite Coatings. *Plasma Processes Polym.* **2009**, *6*, 417–424.

- (9) Polcar, T.; Evaristo, M.; Stueber, M.; Cavaleiro, A. Mechanical and Tribological Properties of Sputtered Mo–Se–C Coatings. *Wear* **2009**, *266*, 393–397.

- (10) Polcar, T.; Gustavsson, F.; Thersleff, T.; Jacobson, S.; Cavaleiro, A. Complex Frictional Analysis of Self-Lubricant W–S–C/Cr Coating. *Faraday Discuss.* **2012**, *156*, 383–401.

- (11) Polcar, T.; Martinez, R.; Vitu, T.; Kopecky, L.; Rodriguez, R.; Cavaleiro, A. High Temperature Tribology of CrN and Multilayered Cr/CrN Coatings. *Surf. Coat. Technol.* **2009**, *203*, 3254–3259.

- (12) Dienwiebel, M.; Verhoeven, G. S.; Pradeep, N.; Frenken, J. W. M.; Heimberg, J. A.; Zandbergen, H. W. Superlubricity of Graphite. *Phys. Rev. Lett.* **2004**, *92*, 126101.

- (13) Grierson, D. S.; Carpick, R. W. Nanotribology of Carbon-Based Materials. *Nano Today* **2007**, *2*, 12–21.

- (14) Klein, H.; Pailharey, D.; Mathey, Y. Friction Force Studies on Layered Materials Using an Atomic Force Microscope. *Surf. Sci.* **1997**, *387*, 227–235.

- (15) Lee, C.; Li, Q. Y.; Kalb, W.; Liu, X. Z.; Berger, H.; Carpick, R. W.; Hone, J. Frictional Characteristics of Atomically Thin Sheets. *Science* **2010**, *328*, 76–80.

- (16) Hu, J.; Xiao, X. D.; Ogletree, D. F.; Salmeron, M. Atomic-Scale Friction and Wear of Mica. *Surf. Sci.* **1995**, *327*, 358–370.

- (17) Kopta, S.; Salmeron, M. The Atomic Scale Origin of Wear on Mica and Its Contribution to Friction. *J. Chem. Phys.* **2000**, *113*, 8249–8252.

- (18) Miyake, S. Atomic-Scale Wear Properties of Muscovite Mica Evaluated by Scanning Probe Microscopy. *Appl. Phys. Lett.* **1994**, *65*, 980–982.

- (19) Miyake, S. 1 nm Deep Mechanical Processing of Muscovite Mica by Atomic-Force Microscopy. *Appl. Phys. Lett.* **1995**, *67*, 2925–2927.

- (20) Park, N. S.; Kim, M. W.; Langford, S. C.; Dickinson, J. T. Atomic Layer Wear of Single-Crystal Calcite in Aqueous Solution Scanning Force Microscopy. *J. Appl. Phys.* **1996**, *80*, 2680–2686.

- (21) Gnecco, E.; Bennewitz, R.; Meyer, E. Abrasive Wear on the Atomic Scale. *Phys. Rev. Lett.* **2002**, *88*, 215501.

- (22) Kim, Y.; Huang, J. L.; Lieber, C. M. Characterization of Nanometer Scale Wear and Oxidation of Transition-Metal Dichalcogenide Lubricants by Atomic Force Microscopy. *Appl. Phys. Lett.* **1991**, *59*, 3404–3406.

- (23) Zhang, X. L.; Celis, J. P. Nanotribology of MoS_x Coatings Investigated by Oscillating Lateral Force Microscopy. *Appl. Surf. Sci.* **2003**, *206*, 110–118.

- (24) Zekonyte, J.; Cavaleiro, A.; Polcar, T. Frictional Properties of Self-Adaptive Chromium Doped Tungsten–Sulfur–Carbon Coatings at Nanoscale. *Appl. Surf. Sci.* **2014**, *303*, 381–387.

- (25) Beake, B. D.; Leggett, G. J.; Alexander, M. R. Characterisation of the Mechanical Properties of Plasma-Polymerised Coatings by Nanoindentation and Nanotribology. *J. Mater. Sci.* **2002**, *37*, 4919–4927.

- (26) Oliver, W. C.; Pharr, G. M. An Improved Technique for Determining Hardness and Elastic-Modulus Using Load and Displacement Sensing Indentation Experiments. *J. Mater. Res.* **1992**, *7*, 1564–1583.

- (27) Hutter, J. L.; Bechhoefer, J. Calibration of Atomic-Force Microscope Tips. *Rev. Sci. Instrum.* **1993**, *64*, 1868–1873.

- (28) Ogletree, D. F.; Carpick, R. W.; Salmeron, M. Calibration of Frictional Forces in Atomic Force Microscopy. *Rev. Sci. Instrum.* **1996**, *67*, 3298–3306.
- (29) Grafstrom, S.; Neitzert, M.; Hagen, T.; Ackermann, J.; Neumann, R.; Probst, O.; Wortge, M. The Role of Topography and Friction for the Image Contrast in Lateral Force Microscopy. *Nanotechnology* **1993**, *4*, 143–151.
- (30) Rumaner, L. E.; Tazawa, T.; Ohuchi, F. S. Compositional Change of (0001) WS₂ Surfaces Induced by Ion-Beam Bombardment with Energies Between 100 and 1500 eV. *J. Vac. Sci. Technol., A* **1994**, *12*, 2451–2456.
- (31) Mullins, D. R.; Lyman, P. F. Sulfur-Induced Changes in the W(001) Surface Core Level Shift. *Surf. Sci.* **1993**, *285*, L473–L478.
- (32) Carpick, R. W.; Ogletree, D. F.; Salmeron, M. A General Equation for Fitting Contact Area and Friction vs Load Measurements. *J. Colloid Interface Sci.* **1999**, *211*, 395–400.
- (33) Carpick, R. W.; Salmeron, M. Scratching the Surface: Fundamental Investigations of Tribology with Atomic Force Microscopy. *Chem. Rev.* **1997**, *97*, 1163–1194.
- (34) Johnson, K. L. Adhesion and Friction Between a Smooth Elastic Spherical Asperity and a Plane Surface. *Proc. R. Soc. London, Ser. A* **1997**, *453*, 163–179.
- (35) Schwarz, U. D.; Allers, W.; Gensterblum, G.; Wiesendanger, R. Low-Load Friction Behavior of Epitaxial C-60 Monolayers Under Hertzian Contact. *Phys. Rev. B: Condens. Matter Mater. Phys.* **1995**, *52*, 14976–14984.
- (36) Schwarz, U. D.; Zworner, O.; Koster, P.; Wiesendanger, R. Quantitative Analysis of the Frictional Properties of Solid Materials at Low Loads. 1. Carbon Compounds. *Phys. Rev. B: Condens. Matter Mater. Phys.* **1997**, *56*, 6987–6996.
- (37) Derjaguin, B. V.; Muller, V. M.; Toporov, Y. P. Effect of Contact Deformations on Adhesion of Particles. *J. Colloid Interface Sci.* **1975**, *53*, 314–326.
- (38) Maugis, D. Adhesion of Spheres: the JKR-DMT Transition Using a Dugdale Model. *J. Colloid Interface Sci.* **1992**, *150*, 243–269.
- (39) Hertz, H. On the Contact of Elastic Solids. *J. Reine Angew. Math.* **1881**, *92*, 156–171.
- (40) Johnson, K. L.; Kendall, K.; Roberts, A. D. Surface Energy and Contact of Elastic Solids. *Proc. R. Soc. London, Ser. A* **1971**, *324*, 301.
- (41) Schwarz, U. D. A Generalized Analytical Model for the Elastic Deformation of an Adhesive Contact Between a Sphere and a Flat Surface. *J. Colloid Interface Sci.* **2003**, *261*, 99–106.
- (42) Grierson, D. S.; Liu, J. J.; Carpick, R. W.; Turner, K. T. Adhesion of Nanoscale Asperities with Power-Law Profiles. *J. Mech. Phys. Solids* **2013**, *61*, 597–610.
- (43) Liu, J. J.; Notbohm, J. K.; Carpick, R. W.; Turner, K. T. Method for Characterizing Nanoscale Wear of Atomic Force Microscope Tips. *ACS Nano* **2010**, *4*, 3763–3772.
- (44) Carpick, R. W.; Agrait, N.; Ogletree, D. F.; Salmeron, M. Variation of the Interfacial Shear Strength and Adhesion of a Nanometer-Sized Contact. *Langmuir* **1996**, *12*, 3334–3340.
- (45) Gotsmann, B.; Lantz, M. A. Atomistic Wear in a Single Asperity Sliding Contact. *Phys. Rev. Lett.* **2008**, *101*, 125501.
- (46) Wang, J. F.; Rose, K. C.; Lieber, C. M. Load-Independent Friction: MoO₃ Nanocrystal Lubricants. *J. Phys. Chem. B* **1999**, *103*, 8405–8409.
- (47) Hansson, P. M.; Claesson, P. M.; Swerin, A.; Briscoe, W. H.; Schoelkopf, J.; Gane, P. A. C.; Thormann, E. Frictional Forces Between Hydrophilic and Hydrophobic Particle Coated Nanostructured Surfaces. *Phys. Chem. Chem. Phys.* **2013**, *15*, 17893–17902.
- (48) Quignon, B.; Pilkington, G. A.; Thormann, E.; Claesson, P. M.; Ashfold, M. N. R.; Mattia, D.; Leese, H.; Davis, S. A.; Briscoe, W. H. Sustained Frictional Instabilities on Nanodomed Surfaces: Stick Slip Amplitude Coefficient. *ACS Nano* **2013**, *7*, 10850–10862.
- (49) Pilkington, G. A.; Thormann, E.; Claesson, P. M.; Fuge, G. M.; Fox, O. J. L.; Ashfold, M. N. R.; Leese, H.; Mattia, D.; Briscoe, W. H. Amontonian Frictional Behaviour of Nanostructured Surfaces. *Phys. Chem. Chem. Phys.* **2011**, *13*, 9318–9326.
- (50) Grosseau-Poussard, J. L.; Moine, P.; Brendle, M. Shear Strength Measurements of Parallel MoS_x Thin Films. *Thin Solid Films* **1997**, *307*, 163–168.
- (51) Bowers, R. C. Coefficient of Friction of High Polymers as a Function of Pressure. *J. Appl. Phys.* **1971**, *42*, 4961–4970.
- (52) Labuda, A.; Hausen, F.; Gosvami, N. N.; Grutter, P. H.; Lennox, R. B.; Bennewitz, R. Switching Atomic Friction by Electrochemical Oxidation. *Langmuir* **2011**, *27*, 2561–2566.
- (53) Filleter, T.; McChesney, J. L.; Bostwick, A.; Rotenberg, E.; Emtsev, K. V.; Seyller, T.; Horn, K.; Bennewitz, R. Friction and Dissipation in Epitaxial Graphene Films. *Phys. Rev. Lett.* **2009**, *102*, 086102.